Journal Pre-proofs

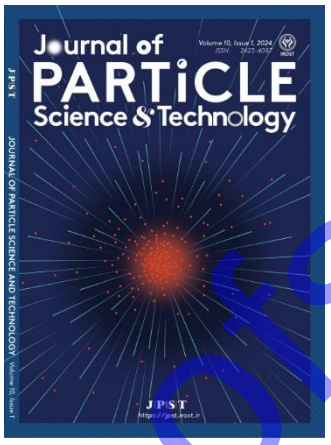

Single-step electrospraying fabrication of composite nanofiltration membranes for efficient bentazone herbicide removal from water

Rezvane Mohammadpour, Razieh Beigmoradi, Abdolreza Samimi, Davod Mohebbi-Kalhori

DOI: https://doi.org/10.22104/jpst.2026.8363.1295
Manuscript number: JPST-2606-1295

To appear in: *Journal of Particle Science and Technology (JPST)*

Received Date: 22 June 2026
Received Date in revised form: 21 July 2026
Accepted Date: 28 July 2026

Please cite this article as: Mohammadpour, R., Beigmoradi, R., Samimi, A., Mohebbi-Kalhori, D., Single-step electrospraying fabrication of composite nanofiltration membranes for efficient bentazone herbicide removal from water, *Journal of Particle Science and Technology* (2025), doi: https://doi.org/10.22104/jpst.2026.8363.1295

Single-step electrospraying fabrication of composite nanofiltration membranes for efficient bentazone herbicide removal from water

Rezvane Mohammadpour[a], Razieh Beigmoradi[b,*], Abdolreza Samimi[a], Davod Mohebbi-Kalhori[a]

[a] *Department of Chemical Engineering, University of Sistan and Baluchestan, Zahedan, Iran*
[b] *Department of Chemical Engineering, Faculty of Engineering, Ardakan University, Ardakan, Iran*

Abstract

A composite nanofiltration membrane was successfully fabricated via a single-step electrospraying process for the efficient removal of bentazone from contaminated water. Key electrospraying parameters—polymer concentration, solution flow rate, and applied electric field strength—were systematically optimized using the Taguchi design of experiments, which identified polymer concentration as the most influential factor governing membrane performance. The optimum fabrication conditions were determined to be a 5 wt% polymer concentration, a 2.2 $mL.h^{-1}$ flow rate, and a 0.66 $kV.cm^{-1}$ electric field strength. The fabricated membranes were characterized using scanning electron microscopy, nitrogen adsorption–desorption, water contact angle, and surface profilometry. Membrane performance was evaluated using a 200 $mg.L^{-1}$ bentazone feed solution in a vacuum-assisted dead-end filtration system operated at a transmembrane pressure of 10 psi. Under these optimal conditions, the membrane exhibited a pure water flux of 34.7 $L.m^{-2}.h^{-1}$. During bentazone filtration, the flux decreased to 19.75 $L.m^{-2}.h^{-1}$, while achieving an excellent bentazone rejection of 96.2 ± 1.44 %. These findings confirm that optimizing electrospraying parameters, particularly polymer concentration, is critical for developing high-performance composite nanofiltration membranes. Overall, the proposed single-step electrospraying method offers a simple, highly controllable, and practical alternative to conventional approaches for fabricating composite nanofiltration membranes.

Keywords: Electrospray deposition, Polyethersulfone support, Composite nanofiltration polyamide membrane, Bentazone rejection

1. Introduction

With the intensification of climate change, global warming, and rapid population growth, the water scarcity crisis has become one of the greatest challenges facing human societies. Globally, the agricultural sector accounts for over 70 % of total freshwater withdrawals, making it the largest consumer of freshwater resources [1-3]. In parallel, the uncontrolled release of industrial and municipal wastewater into the environment has intensified the contamination of surface water and groundwater resources, posing serious environmental and public health concerns. These challenges associated with water scarcity have made water reuse and advanced wastewater treatment essential components of sustainable water management [1].

One of the major challenges in water treatment is the limited effectiveness of conventional treatment processes, such as coagulation, sedimentation, and adsorption, in eliminating persistent micropollutants, including pesticides and herbicides. These contaminants are often resistant to biodegradation and may persist in aquatic environments for extended periods, even at trace concentrations [4-7].

Although advanced oxidation processes (AOPs), including ultrasound, ozonation, Fenton-based reactions, and photocatalysis, have been widely studied for the degradation of toxic contaminants [5,8,9], their large-scale application is still limited by operational complexity, high capital and operating costs, and substantial chemical consumption.

Among these contaminants, bentazone is recognized as a highly soluble and persistent herbicide that is widely used in the cultivation of key crops, including rice, corn, and soybean [10-12]. Owing to its high-water solubility, bentazone has a strong tendency to leach into groundwater aquifers. Reports from the United States Environmental Protection Agency (US EPA) and the World Health Organization (WHO) have confirmed the increasing occurrence of bentazone in water resources, leading to the establishment of stringent regulatory limits for its concentration in drinking water [13]. Furthermore, recent studies have indicated that long-term exposure to bentazone may pose significant

risks to the stability and ecological balance of aquatic ecosystems [14-16].

Among membrane-based separation technologies, nanofiltration (NF) has gained broad acceptance as an effective and sustainable approach for removing agricultural micropollutants, including bentazone [10-12,17-19]. Within this category, composite NF membranes are of particular significance because they integrate the advantageous properties of different constituent materials, enabling superior water permeability, high separation selectivity, improved mechanical and chemical stability, and enhanced resistance to membrane fouling [20].

These characteristics make them particularly attractive for sustainable water treatment applications requiring both high contaminant rejection and operational efficiency. Nevertheless, simultaneously achieving high water permeability and excellent separation performance remains a persistent challenge, as both properties are strongly governed by membrane morphology, pore architecture, and surface characteristics. Consequently, considerable research efforts have been devoted to developing fabrication strategies capable of precisely controlling these structural features while maintaining simple, reproducible, and scalable manufacturing processes. Despite the remarkable separation performance of composite nanofiltration membranes [20,21], many reported fabrication routes still rely on multistep procedures involving surface modification, pore architecture engineering, or post-fabrication functionalization to achieve the desired membrane properties. Such approaches inevitably increase manufacturing complexity, processing time, solvent consumption, and production costs while limiting reproducibility and large-scale implementation. Therefore, the development of simple, controllable, and efficient fabrication techniques capable of producing high-performance NF membranes in a single step remains an important research objective [20,22,23].

Among the various fabrication techniques proposed for composite nanofiltration membranes, electrospraying has emerged as a particularly attractive approach due to its ability to precisely control membrane morphology, pore architecture, and surface characteristics through a simple single-step process [24-27]. Unlike conventional fabrication routes that often require multiple processing stages

or post-fabrication surface modification, electrospraying enables the direct deposition of polymeric materials onto porous support substrates, thereby simplifying membrane fabrication, reducing solvent-intensive processing steps, and minimizing overall solvent consumption [25]. Moreover, the versatility of electrospraying in regulating solution composition and processing parameters provides an effective platform for tailoring membrane microstructure and optimizing separation performance. Its capability to form functional polymer layers on a wide range of porous support materials further enhances its flexibility for the design and fabrication of advanced composite nanofiltration membranes with high Despite these advances, previous studies have primarily employed electrospraying as an auxiliary technique for membrane fabrication, including surface modification, nanoparticle deposition, or the formation of polymer selective layers through electrosprayed interfacial polymerization (EIP) [26,28]. To the best of the authors' knowledge, its application as a standalone, single-step fabrication strategy for directly producing polyamide nanofiltration membranes from polymer solutions has received very limited attention.

Therefore, the present study aimed to fabricate a polyamide nanofiltration membrane by directly depositing a polymer solution onto a polyethersulfone (PES) support through a single-step electrospraying process, thereby eliminating the need for multistep surface modification or interfacial polymerization. To establish a simple and controllable fabrication strategy, the effects of key processing parameters, including polymer solution concentration, applied electric field strength, and solution flow rate, were systematically optimized using the Taguchi design of experiments. The fabricated membranes were subsequently characterized in terms of their morphology, pore structure, surface topography, and wettability using scanning electron microscopy (SEM), nitrogen adsorption–desorption analysis, surface profilometry, and water contact angle measurements. Finally, the separation performance of the fabricated membranes was evaluated through pure water permeation and bentazone filtration.

2. Experimental

2.1. Materials

Polyamide 6 (PA6) was purchased from CASA Polymer Solutions GbR (Germany). Formic acid (FA, 98–100 wt%), as solvent, and bentazone were obtained from Merck (Germany) and Aria Shimi (Iran), respectively. a commercial micro-filter (Millipore Sigma, USA, pore size: 0.45 μm, diameter: 90 mm, hydrophilic) was used as the support layer. According to the datasheet, the pure water flux of the membrane was reported to be approximately 217 $L.m^{-2}.h^{-1}$ at an operating pressure of 10 psi. Deionized water with a resistivity higher than 18 MΩ.cm was produced using a Milli-Q Direct water purification system (Merck Millipore, Germany). All chemicals were used as received without any further purification.

2.2. Electrospraying procedure

The electrospraying apparatus consisted of a plastic syringe, a stainless-steel needle (16G), a micro infusion pump (WZ-60C2, China), an extractor ring, an aluminum foil collector, and a high-voltage power supply (LD Didactic GmbH, Germany) supplying an output voltage range of 0–25 kV. A schematic diagram of the vertical electrospray experimental setup is illustrated in Fig. 1. A positive voltage was applied to the polymer solution, and the spinneret-to-collector distance was adjusted to maintain a constant electric field strength. To identify the optimal electrospraying process conditions, three parameters at three levels, polymer solution concentration (3, 4, and 5 %wt), electric field strength (0.66,0.84, 0.91 $kV.cm^{-1}$), and flow rate (0.9, 1.2, 2.2 $mL.h^{-1}$), were set in accordance with the L^9 orthogonal array of the Taguchi design-of-experiments methodology. The parameter ranges were selected based on preliminary experiments and previous studies reported in the literature [29-31]. Since the primary objective of this study was to optimize the electrospraying fabrication process rather than the membrane separation performance directly, the mean diameter of the electrosprayed particles was selected as the response variable. This structural parameter was considered suitable

because it governs the formation, uniformity, and compactness of the deposited selective layer, which are expected to influence the final membrane performance.

The polymer solutions were prepared by dissolving polyamide in formic acid, and stirred at room temperature for 24 hours to ensure complete dissolution.

After determining the optimal conditions of the electrospraying process, the polyamide layer was deposited onto the PES support membrane. The resulting NF membrane was then immersed in deionized water for 48 hours to ensure complete removal of residual solvent, after which it was prepared for subsequent characterization and testing.

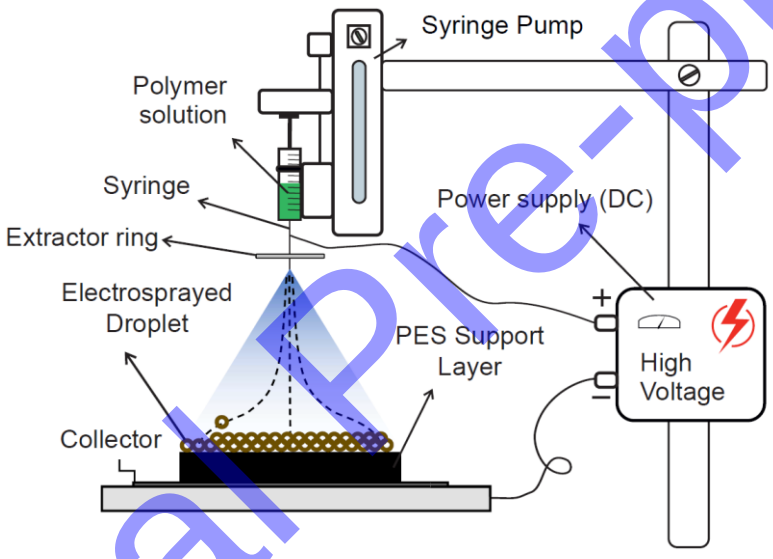

Fig. 1. Schematic representation of the experimental apparatus used for the vertical electrospray process, illustrating the syringe pump, high-voltage power supply, needle, extractor ring, and collector.

2.3. Characterization techniques

The morphology of the PA layer was evaluated using SEM (KYKY-EM3900M, China). Before SEM observations, the samples were sputter-coated with a thin gold layer. The average diameter of the electrosprayed dried particles as coating particles on the target was estimated using image analysis software (ImageJ; http://rsb.info.nih.gov/ij/, National Institutes of Health, USA). The thickness was measured using a digital micrometer (accuracy: 1 μm; Asimeto, Japan). The wettability of the NF membrane surface was evaluated by water contact angle measurements (Yasin Pajooh, Iran).

Topographies and roughness of the textured NF membrane surface was acquired by an Profilometer (LPM-D2, Fanavari. Kahroba, Iran) in air. The pore size and porosity of the NF membrane were determined from nitrogen adsorption–desorption isotherms using the Brunauer–Emmett–Teller (BET) method, and the pore size distribution was further analyzed by the Barrett–Joyner–Halenda (BJH) method (BELSORP-mini II, BEL Japan).

The filtration performance of the fabricated NF membrane was evaluated using a laboratory-scale vacuum-assisted dead-end filtration system equipped with a glass membrane holder, a vacuum flask, and a vacuum pump [29]. The system was operated at a transmembrane pressure of 10 psi, and the permeate flux (Equation (1)) and bentazone rejection were determined.

The concentration of bentazone in the permeate was measured by a UV-Vis spectrophotometer in the wavelength range of 200–800 nm.

$$J = \frac{V}{At} \tag{1}$$

In the equation (1), J represents the permeate flux in $L.m^{-2}.h^{-1}$ (LMH); V represents permeate volume in (L); A represents the effective membrane area in (m^2); and t represents the time the liquid passed through the membrane (h).

3. Results and Discussion

3.1. Morphological analysis by SEM

The SEM images of the electrosprayed products from nine experimental runs, carried out according to the designed conditions, are shown in Fig. 2. Image analysis was performed to calculate the mean individual particle diameter for each sample, which was then employed as the response variable to identify the optimal processing conditions (Table 1). Preliminary observations indicated that low concentrations led to operational instability in the electrospray process, regardless of adjustments

made to the electric field and flow rate. This instability was accompanied by the intermittent production of oversize particles, ultimately increasing the mean diameter. Consequently, the Taguchi experimental design was implemented, and the signal-to-noise (*S/N*) ratio was employed as the response parameter to optimize the process conditions.

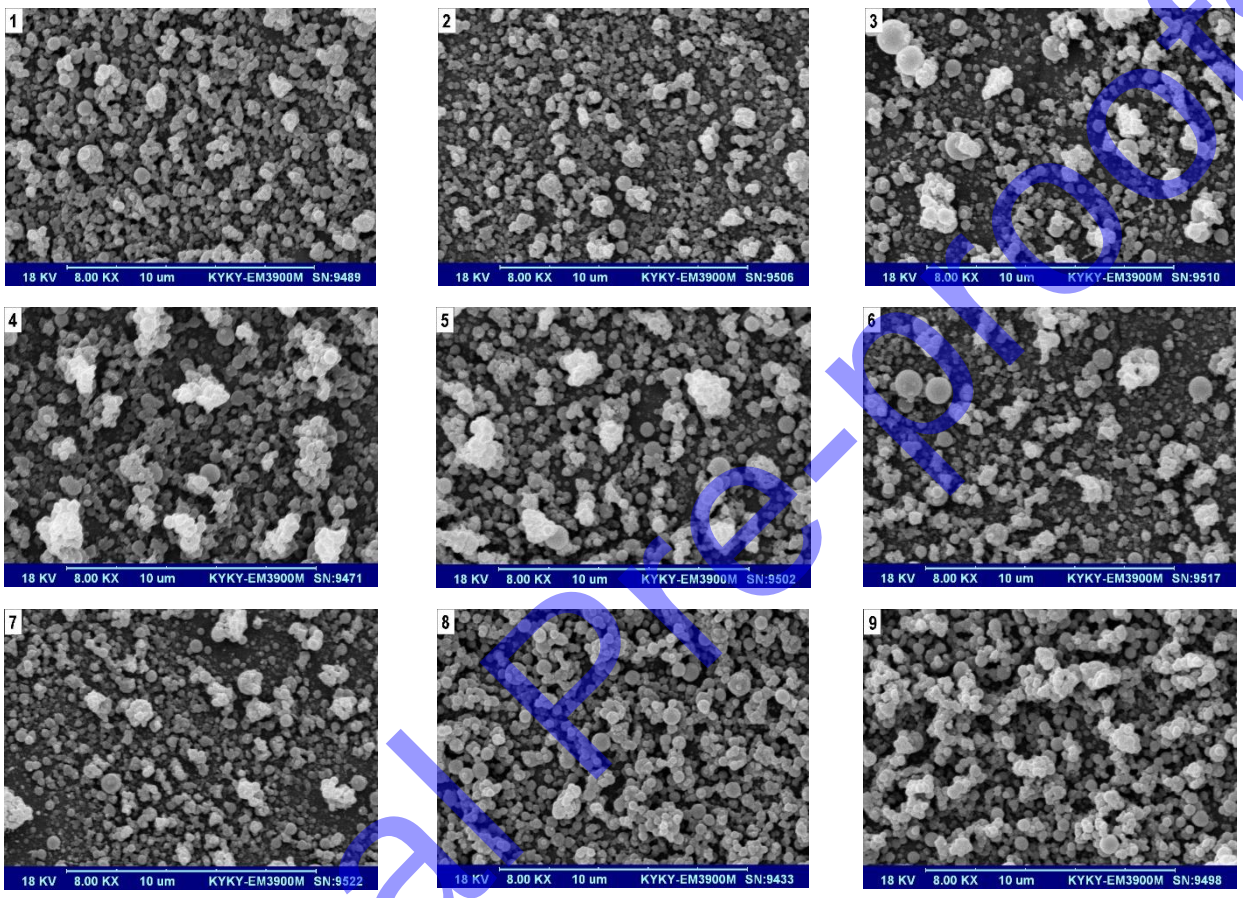

Fig. 2. SEM Micrographs of the electrosprayed particles morphology produced under nine Taguchi-designed experimental conditions.

The main effects of the three process parameters on the mean of means and the mean of S/N ratios are presented in Figs. 3 and 4, respectively. In both figures, electric field strength ($kV.cm^{-1}$) and concentration (wt%) are clearly the dominant factor, exhibiting the largest variation in the response across its levels. In contrast, flow rate ($mL.h^{-1}$) shows the smallest variation, indicating that its influence on the response is minor within the tested ranges. The *S/N* ratios were calculated based on the smaller-the-better quality characteristic, as the goal was to minimize the response variable.

Table 1. Experimental conditions and the resulting mean particles diameter for nine electrospraying experiments.

Run	Concentration (wt%)	Flow rate ($mL.h^{-1}$)	Electric field strength ($kV.cm^{-1}$)	Particles' average diameter (nm)
1	3	0.9	0.66	308±80
2	3	1.2	0.84	338±85
3	3	2.2	0.91	323±16
4	4	0.9	0.84	351±75
5	4	1.2	0.91	328±13
6	4	2.2	0.66	281±50
7	5	0.9	0.91	264±34
8	5	1.2	0.66	256±30
9	5	2.2	0.84	296±42

The S/N ratio for each trial was computed using the following Equation (2) [32].

$$S/N = -10 \times \mathrm{Log}_{10}\left(\frac{1}{n}\sum_{i}^{n} y_i\right) \quad (2)$$

where y_i represents the measured response for the i-th replication and n is the number of replications per experimental run.

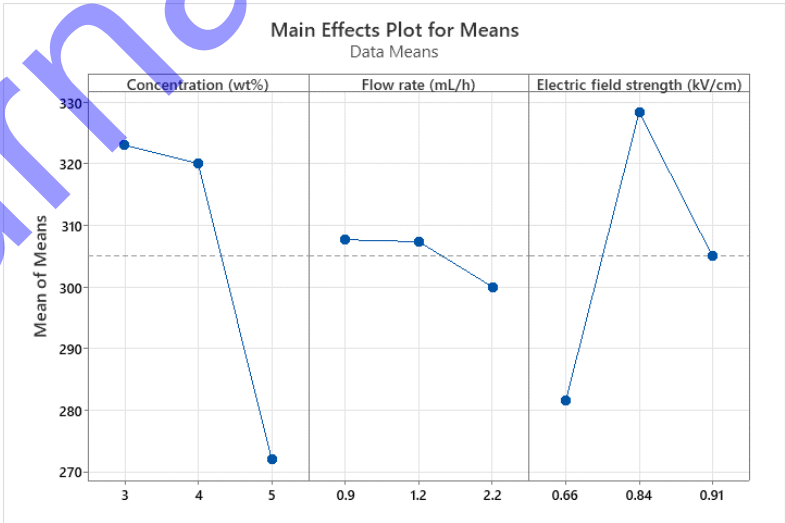

Fig. 3. Main effects plot for the mean of means. The effects of concentration (wt%), flow rate ($mL.h^{-1}$), and electric field strength ($kV.cm^{-1}$) on the mean of means are shown.

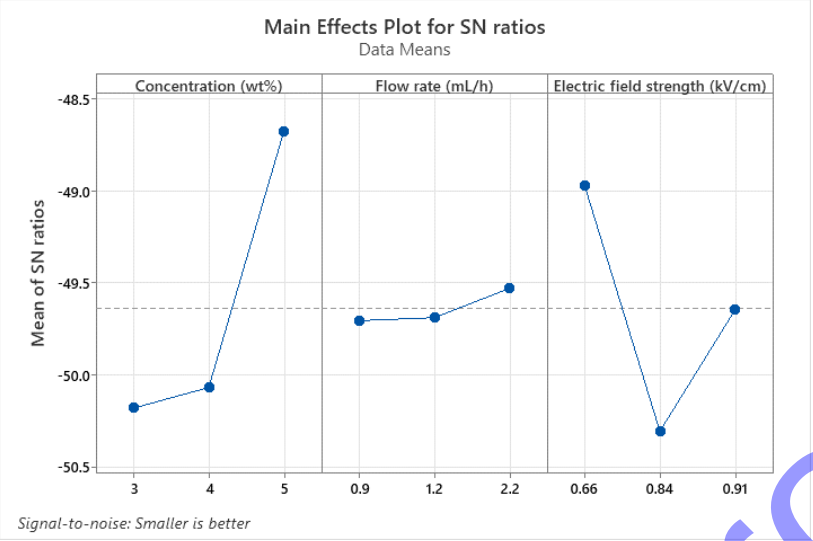

Fig. 4. Main effects plot for the mean of S/N ratios (Smaller-is-better). The effects of concentration (wt%), flow rate (mL.h^{-1}), and electric field strength (kV.cm^{-1}) on the mean S/N ratio are illustrated.

The optimal process parameters for minimizing the response variable (smaller-is-better) were determined using the main effects plots shown in Figs. 3 and 4. In both plots, the lowest mean of means (Fig. 3) and the highest signal-to-noise ratio (Fig. 4) were consistently achieved at the same factor levels: concentration of 5 wt%, flow rate of 2.2 mL.h^{-1}, and electric field strength of 0.66 kV.cm^{-1}. This agreement between the two criteria indicates that the selected combination simultaneously minimizes the average response and maximizes process robustness. The lower mean of means corresponds to the smallest achievable particle diameter, while the higher *S/N* ratio reflects reduced sensitivity to uncontrollable noise factors. Consequently, the condition comprising 5 wt% concentration, 2.2 mL.h^{-1} flow rate, and 0.66 kV.cm^{-1} electric field strength is identified as the overall optimal setting for producing the smallest and most consistent particle diameter. Based on the Taguchi design of experiments, Equation (3a) was used to predict the optimal nanofiber diameter and to evaluate whether the selected optimal levels can produce the desired fiber diameter [33].

$$Y_{opt} = \frac{T}{N} + (\bar{A}_3 - \frac{T}{N}) + (\bar{B}_3 - \frac{T}{N}) + (\bar{C}_1 - \frac{T}{N}) \quad (3a)$$

$$\frac{T}{N} = \frac{\sum_{i=1}^{9}(S/N)_i}{9} \quad (3b)$$

where Y_{opt} is the predicted optimal particles' diameter, *T/N* is the overall mean of the *S/N* ratios (Equation (3b)), and $\bar{A}_3$, $\bar{B_3}$, and $\bar{C_1}$ are the *S/N* ratios at the optimal levels of concentration, flow rate, and electric field strength, respectively. Based on the Taguchi prediction formula (Equation (3a)), the optimal particles' diameter was calculated to be 243.67 nm. Accordingly, the separation layer was fabricated under the optimal conditions, i.e., a concentration of 5 wt%, a flow rate of 2.2 $mL.h^{-1}$, and an electric field strength of 0.66 $kV.cm^{-1}$, to evaluate the predicted optimum.

Fig. 5 presents the SEM image of the polyamide surface membrane fabricated under the optimal parameter set. The main image illustrates the overall surface morphology of the electrosprayed separation layer, revealing a dense and uniform structure without visible pores or defects. A higher-magnification view is provided as an inset in the lower corner of Fig. 5, enabling improved resolution for individual particle visualization and more accurate diameter measurements. Using image analysis software, the diameters of at least 40 randomly selected particles were measured, yielding an average diameter of 247 ± 50 nm. This finding reveals acceptable agreement between the calculated and experimental values, thereby supporting the validity of the optimization approach.

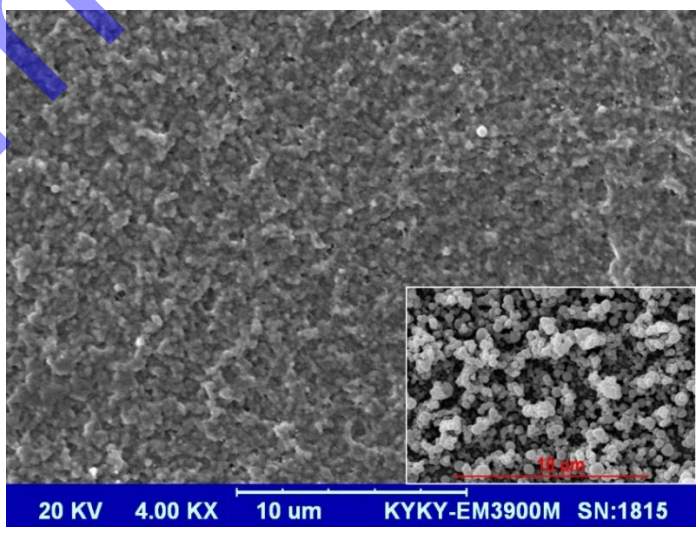

Fig. 5. SEM image of the membrane fabricated under optimal conditions (inset: magnified view).

3.2. Surface hydrophilicity and roughness

Water contact angle measurements were performed to evaluate the surface wettability of the pristine PES support and the fabricated NF membrane. The pristine PES support exhibited a mean contact angle of 74 ± 0.8°, while the fabricated NF membrane showed a comparable value of 74 ± 0.3° (Fig. 6(a)). The negligible difference between the two measurements confirms that the single-step electrospraying process did not significantly alter the surface wettability after the formation of the polyamide layer. This observation is noteworthy, as previous studies have reported that electrospraying can modify membrane surface characteristics, including increasing surface roughness and reducing surface energy, which may enhance hydrophobicity in specific membrane applications. In contrast, the present electrospraying strategy enabled the formation of a polyamide selective layer while preserving the inherent wettability of the PES support, without requiring hydrophilic additives or post-fabrication surface modification. Given that surface topography is closely related to membrane morphology and can influence membrane performance, the surface characteristics of the fabricated NF membrane were further evaluated using profilometry. The profilometry results revealed an average surface roughness (*Ra*) of 38 ± 0.9 nm (Figs. 6(b), 6(c)), indicating the formation of a relatively smooth and uniform surface structure after the electrospraying process. This observation is consistent with the contact angle results, demonstrating that the single-step electrospraying approach enabled the formation of a homogeneous polyamide layer while preserving the surface wettability of the PES support. The relatively smooth and uniform surface morphology further confirms the capability of electrospraying to provide controlled surface characteristics without requiring additional surface modification steps.

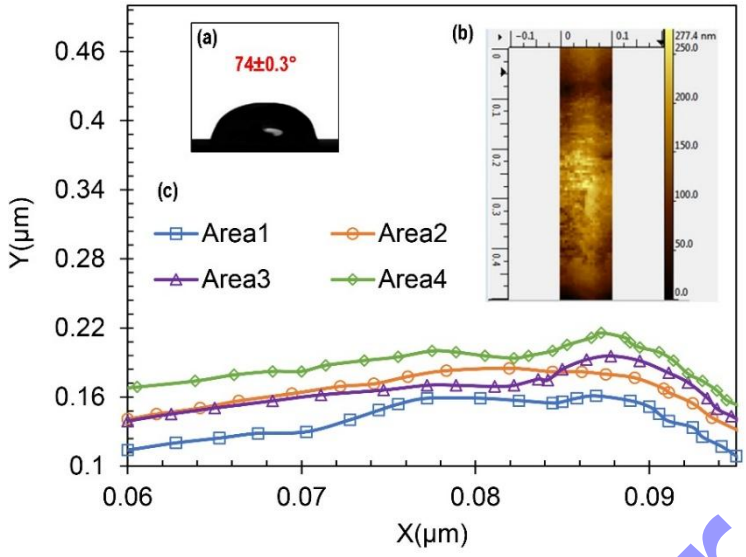

Fig. 6. Surface characterization of the electrosprayed membrane. (a) Water contact angle. (b) 2D profilometry image of the membrane surface. (c) Surface roughness variation across four random areas.

3.3. Nitrogen adsorption-desorption isotherm and pore size distribution

Fig. 7(a) illustrates the nitrogen adsorption-desorption hysteresis loop obtained from the overall membrane structure, which was used to evaluate its pore geometry and size distribution. According to the IUPAC classification, the resulting isotherm corresponds to Type II behavior with an H3-type hysteresis loop [34]. The absence of a distinct saturation plateau at elevated relative pressures, combined with the non-rigid nature of the hysteresis loop, suggests the presence of slit-shaped pores and interparticle voids—features that are consistent with the layered packing morphology expected from the electrospray deposition process. To gain deeper insight into this pore architecture, the corresponding BJH pore size distribution was evaluated from the adsorption branch (Fig. 7(b)). The profile exhibits a prominent intensity peak at the lower measurement limit ($r_p \sim 1.2$ nm), followed by a sharp exponential decay. This trend demonstrates that the membrane's porosity is predominantly dominated by ultra-small pores within the micro- to narrow meso-pore region ($r_p < 3$ nm), with a negligible contribution from larger macroscopic voids. Quantitatively, the BJH analysis yielded a total pore volume of 0.73 $cm^3.g^{-1}$, a specific surface area of 3.18 $m^2.g^{-1}$, and an average pore diameter of 11.17 nm. The coexistence of a relatively low specific surface area alongside a high total pore

volume is characteristic of the overall membrane structure. Given that the BJH analysis was performed on the complete membrane assembly, the macro porous PES support layer—owing to its substantial thickness and intrinsic porosity—dominates the measured specific surface area and total pore volume. In contrast, the thin PA6 selective layer deposited on top contributes negligibly to these bulk values. The calculated average pore diameter of 11.17 nm—which is substantially higher than the primary pore size peak at approximately 1.2 nm—reflects the volume-weighted averaging of the entire pore system, wherein the larger pores of the underlying PES support exert a significant mathematical weighting on the mean value, despite the majority of pores residing in the sub-3 nm regime. This interpretation is fully consistent with the electrospray deposition process, wherein PA6 particles, upon rapid solvent evaporation and solidification, form a layered structure primarily at the entrances of the support pores, rather than filling or penetrating the macro porous network beneath. The resulting dense PA6 layer on the PES support surface effectively acts as a selective barrier. This behavior is characteristic of a self-limiting electrospray deposition (ESD) mechanism [27,28]. The self-limiting behavior arises when charge accumulation on the deposited insulating polyamide film repels incoming charged droplets, establishing a maximum film thickness [26]. The characteristics of PA6, including its glassy nature, appear to influence this deposition behavior. This electrostatic repulsion effectively forces the highly charged polymeric species to spread uniformly and pack tightly into a dense, layer-by-layer configuration (schematically depicted in Fig. 1). Consequently, the interparticle voids within this ordered self-limiting assembly are restricted to the sub-3 nm regime. The claim that this dense PA6 layer acts as a barrier at the pore entrances—without clogging the underlying support pores—and enables effective separation for bentazone solutions will be further investigated in the next section through permeate flux and rejection measurements.

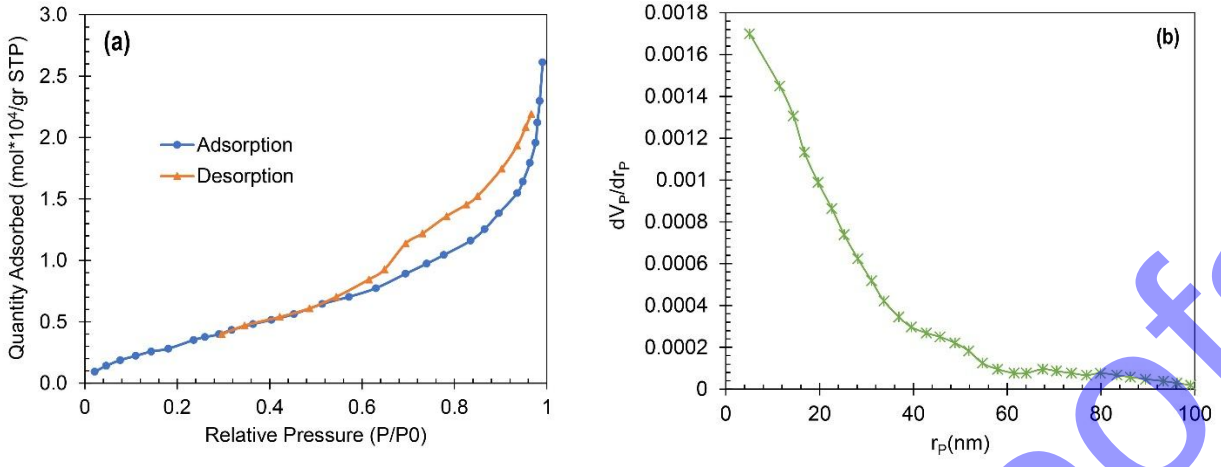

Fig. 7. (a) Nitrogen adsorption–desorption hysteresis loop of the composite NF membrane, exhibiting Type II/H3 behavior; (b) corresponding BJH pore size distribution plot.

3.4. Membrane performance evaluation

UV–Vis spectroscopy was employed to assess membrane performance (Fig. 8). The recorded spectra displayed characteristic absorption bands of bentazone, with two principal absorption maxima at 220–230 nm and 330–340 nm. Previous studies [35,36] have shown that the absorption band in the 220–230 nm region provides higher sensitivity for bentazone quantification. Therefore, absorbance values within this wavelength range were used to determine bentazone concentrations and calculate membrane rejection. An additional absorbance band was observed near 278 nm. According to previous reports, this band may correspond to degradation products of bentazone, such as hydroxy- and keto-derivatives, rather than the parent compound itself. Consequently, absorbance at 278 nm was not considered for bentazone quantification. Using calibration curves obtained from standard bentazone solutions, the rejection efficiency of the fabricated membrane was determined to be 96.2 ± 1.44 %. The pure water flux of the membrane was 34.7 $L.m^{-2}.h^{-1}$, whereas the flux measured for the bentazone solution decreased to 19.75 $L.m^{-2}.h^{-1}$.

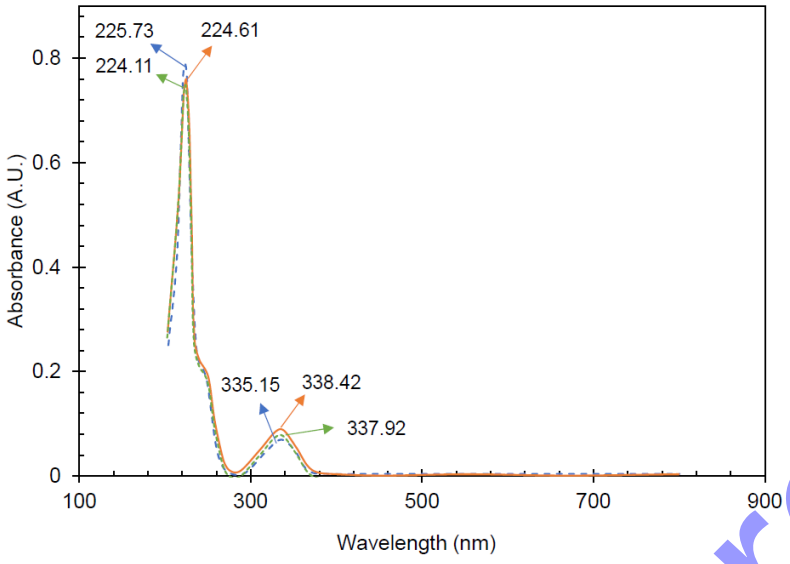

Fig. 8. UV–vis. spectra of residual bentazone in the permeate after filtration. All filtration experiments were performed in triplicate, and the results are reported as mean values.

4. Conclusion

A polyamide NF membrane was successfully fabricated on a PES support through a single-step electrospraying process. The Taguchi design method was employed to optimize the key electrospraying parameters, including polymer solution concentration, applied electric field strength, and solution flow rate, using the mean diameter of deposited polyamide particles as the structural optimization criterion. This structure-oriented optimization strategy enabled the formation of a uniform and compact polyamide selective layer with nanoscale porous characteristics. Morphological analyses confirmed the controlled deposition and homogeneous assembly of polyamide structures, while filtration experiments demonstrated high bentazone rejection (> 95 %) together with satisfactory permeate flux under low operating pressure conditions. The proposed single-step electrospraying approach provides a simple and controllable fabrication route for preparing polyamide nanofiltration membranes, reducing fabrication complexity and minimizing the need for additional surface modification steps. Overall, these findings highlight the potential of electrospraying as an effective strategy for the development of high-performance composite nanofiltration membranes for water treatment applications.

References

[1] A. Panagopoulos and P. Michailidis, "embrane technologies for sustainable wastewater treatment: Advances, challenges, and applications in zero liquid discharge (zld) and minimal liquid discharge (mld) systems, *Membranes,* vol. 15, no. 2, p. 64, 2025.

[2] S. Kim *et al.*, Removal of contaminants of emerging concern by membranes in water and wastewater: An updated review, *Environmental Engineering Research,* vol. 30, no. 1, 2025.

[3] J. D. Putuhena, Evaluating the impact of climate change on freshwater resources: a remote sensing approach for global water scarcity assessment, *The Journal of Academic Science,* vol. 1, no. 5, pp. 622-629, 2024.

[4] S. Gavrilaș, T. Gerőcs, B.-D. Chereji, and F.-D. Munteanu, Trends in Advanced Wastewater Treatment Technologies: From Membrane Bioreactors to Advanced Oxidation Processes, *Water,* vol. 18, no. 3, p. 350, 2026.

[5] U. Hübner *et al.*, Advanced oxidation processes for water and wastewater treatment–Guidance for systematic future research, *Heliyon,* vol. 10, no. 9, 2024.

[6] A. Moreira and M. V. da Silva, Exposure to Pesticides, Risk Assessment and Analysis of Occupational Health and Safety in Agriculture Context: A Systematic Review, *Occupational and Environmental Safety and Health VI: Volume 1: Occupational Risk Assessment, Management and Case Studies,* pp. 119-135, 2025.

[7] J. F. Nure and T. T. Nkambule, The recent advances in adsorption and membrane separation and their hybrid technologies for micropollutants removal from wastewater, *Journal of Industrial and Engineering Chemistry,* vol. 126, pp. 92-114, 2023.

[8] M. Priyadarshini, I. Das, M. M. Ghangrekar, and L. Blaney, Advanced oxidation processes: Performance, advantages, and scale-up of emerging technologies, *Journal of Environmental Management,* vol. 316, p. 115295, 2022.

[9] A. Tufail, W. E. Price, and F. I. Hai, A critical review on advanced oxidation processes for the

removal of trace organic contaminants: A voyage from individual to integrated processes, *Chemosphere,* vol. 260, p. 127460, 2020.

[10] J. Ali *et al.*, A mixed matrix polyimide ultrafiltration membrane for efficient removal of bentazon from water, *Chemical Engineering Journal,* vol. 433, p. 134596, 2022.

[11] M. Nematzadeh, A. Samimi, S. Shokrollahzadeh, and D. Mohebbi-Kalhori, Bentazon removal from aqueous solution by reverse osmosis; optimization of effective parameters using response surface methodology, *Advances in Environmental Technology,* vol. 5, no. 4, pp. 193-201, 2019.

[12] Utzeri, G., Guirado-Moreno, J. C., Cova, T. F. G. G. *et al.*, Reusable and effective polyacrylic membranes for mecoprop and bentazon extractions, *npj Clean Water,* vol. 7, no. 1, p. 39, 2024.

[13] F. Edition, Guidelines for drinking-water quality, *WHO Chronicle,* vol. 38, no. 4, pp. 104-8, 2011.

[14] D. Grillo-Avila *et al.*, Effects of the herbicide bentazone on the structure of plankton and benthic communities representative of Mediterranean coastal wetlands: a mesocosm experiment, *Hydrobiologia,* vol. 852, no. 10, pp. 2709-2728, 2025.

[15] A. Oros, Bioaccumulation and trophic transfer of heavy metals in marine fish: Ecological and ecosystem-level impacts, *Journal of Xenobiotics,* vol. 15, no. 2, p. 59, 2025.

[16] S. Kumar and S. Vats, Ecological threats of biomagnification: insights from recent studies, *World Journal of Pharmaceutical Research,* vol. 13, no. 15, pp. 761-771, 2024.

[17] J. B. Moreira, T. D. Santos, M. Zaparoli, A. C. A. de Almeida, J. A. V. Costa, and M. G. de Morais, An overview of nanofiltration and nanoadsorption technologies to emerging pollutants treatment, *Applied Sciences,* vol. 12, no. 16, p. 8352, 2022.

[18] I. F. Farah, Pesticides in surface and groundwater: occurrence, environmental and human health risk, and removal efficiency by membrane technologies, 2025.

[19] B. Zhou *et al.*, Micropollutants removal from aquaculture water using layer-by-layer self-assembled nanofiltration membranes, *Water Research,* vol. 271, p. 122933, 2025.

[20] D. Namla, M. Oves, M. A. Alshaeri, S. M. Al-Maaqar, H. N. Y. Issa, and G. Mangse, Nanofiltration as an advanced wastewater treatment technique: a comprehensive review, *Discover Applied Sciences,* vol. 7, no. 4, p. 355, 2025.

[21] N. Maroufi and N. Hajilary, Nanofiltration membranes types and application in water treatment: a review, *Sustainable Water Resources Management,* vol. 9, no. 5, p. 142, 2023.

[22] H. Yin, D. Wang, M. Shi, and X. Xu, Wastewater treatment and resource recovery by loose nanofiltration membrane: A critical review, *Environmental Engineering Research,* vol. 31, no. 1, p. 250122, 2025.

[23] M. R. Chowdhury, J. Steffes, B. D. Huey, and J. R. McCutcheon, 3D printed polyamide membranes for desalination, *Science,* vol. 361, no. 6403, pp. 682-686, 2018.

[24] T. Ravindran, Electrospray Printing: An Advanced Technique for Processing Polymers into Thin Films for Membrane Applications, 2020.

[25] B. Al-Ghafri, H. H. Kyaw, M. Al-Abri, and W.-J. Lau, Performance study of novel PES membrane using electrospray deposition method for organic contaminants separation, *Chemical Engineering Research and Design,* vol. 186, pp. 73-81, 2022.

[26] R. A. Green-Warren *et al.*, Self-limiting electrospray deposition (SLED) of porous polyimide coatings as effective lithium-ion battery separator membranes, *RSC Applied Polymers,* vol. 2, no. 6, pp. 1074-1081, 2024.

[27] D. A. Kovacevich *et al.*, Self-limiting electrospray deposition for the surface modification of additively manufactured parts, *ACS applied materials & interfaces,* vol. 12, no. 18, pp. 20901-20911, 2020.

[28] L. Lei *et al.*, Obtaining thickness-limited electrospray deposition for 3D coating, *ACS Applied Materials & Interfaces,* vol. 10, no. 13, pp. 11175-11188, 2018.

[29] R. Beigmoradi, A. Samimi, and D. Mohebbi-Kalhori, Fabrication of polymeric nanofibrous mats with controllable structure and enhanced wetting behavior using one-step electrospinning,

Polymer, vol. 143, pp. 271-280, 2018.

[30] H. Moghadam, M. Samimi, A. Samimi, and M. Khorram, Electro-spray of high viscous liquids for producing mono-sized spherical alginate beads, *Particuology,* vol. 6, no. 4, pp. 271-275, 2008.

[31] A. Tabeei, A. Samimi, M. Khorram, and H. Moghadam, Study pulsating electrospray of non-Newtonian and thixotropic sodium alginate solution, *Journal of Electrostatics,* vol. 70, no. 1, pp. 77-82, 2012.

[32] D. C. Montgomery, *Design and Analysis of Experiments*. John wiley & sons, 2017.

[33] R. K. Roy, *A Primer on the Taguchi Method*. Society of Manufacturing Engineers, 2010.

[34] M. Thommes *et al.*, Physisorption of gases, with special reference to the evaluation of surface area and pore size distribution (IUPAC Technical Report), *Pure and Applied Chemistry,* vol. 87, no. 9-10, pp. 1051-1069, 2015.

[35] C. S. Braga *et al.*, Photocatalytic Degradation of Bentazon Pesticide by a Fe 2 O 3-TiO 2 Composite Catalyst Irradiated by UVA, UVB, and Natural Light, *Journal of the Brazilian Chemical Society,* vol. 34, pp. 1284-1292, 2023.

[36] J. Jin, X. Sun, G. Yu, H. Wang, and S. Zhang, Characterization of Bentazone in Potable Water by Combined UV-Visible Spectroscopy, in *2025 IEEE 7th International Conference on Artificial Intelligence, Computer Science, and Information Processing (AICSIP)*, 2025: IEEE, pp. 1-5.